are accurately described by the linear equations (1) by using the technique of Ref. 4. There, curvilinear axes are introduced in which the equations of motion and their solution again have exactly the same form as given here.

References

[1] Schneider, A. M., Prussing, J. E., and Timin, M. E., "A Manual Method for Space Rendezvous Navigation and Guidance," *Journal of Spacecraft and Rockets*, Vol. 6, No. 9, Sept. 1969, pp. 998–1006.

[2] Schneider, A. M., Prussing, J. E., and Timin, M. E., "Manual Techniques for Space Rendezvous and Reentry, Volumes I and II," Technical Rept. AFAL-TR-68-300, Air Force Avionics Laboratory, Wright-Patterson Air Force Base, Ohio, Nov. 1968.

[3] Schneider, A. M. and Koble, H. M., "A Simple Linear Approximation for Perturbed Motion about Moderately Elliptic Orbits," *AIAA Journal*, Vol. 8, No. 10, Oct. 1970, pp. 1903–1905.

[4] Schneider, A. M., "An Improved Deterministic Method for Finding Relative Orbital State from Angle Measurements," Rept. SDC 3-70, Jan. 1970, Department of the Aerospace and Mechanical Engineering Sciences, University of California at San Diego, La Jolla, Calif.

Thrust-Minus-Drag Optimization by Base Bleed and/or Boattailing

A. L. Addy*

University of Illinois at Urbana-Champaign, Urbana, Ill.

Nomenclature

$A,\bar{A}$	=	area; area ratio, A/A_{2E}, respectively
$\bar{B}_0$	=	base bleed-to-nozzle mass flow-rate ratio
C_D	=	afterbody-base drag coefficient = $C_{DB} + C_{DBT}$
C_{DBT},C_{DB}	=	boattail and base drag coefficients, respectively
F_{NET}	=	thrust-minus-drag force
$\bar{L}$	=	boattail length-to-body radius ratio
M	=	Mach number
$P,\bar{P}$	=	absolute pressure; static-to-freestream pressure ratio, P/P_E, respectively
$\bar{\mathcal{R}}_I$	=	ratio of gas constants, $\mathcal{R}_I/\mathcal{R}_E$
V	=	velocity magnitude
X,R	=	longitudinal and radial coordinates, respectively
ρ	=	density
γ	=	ratio of specific heats
β	=	flow angle
ΔC_F	=	incremental thrust-minus-drag coefficient, Eq. (6)

Subscripts

B,BT	=	base and boattail regions, respectively
E,I	=	external (freestream) and internal (nozzle) flows, respectively
R	=	reference configuration
X	=	component in the longitudinal direction
0	=	stagnation conditions
1	=	geometric separation point at terminus of nozzle or afterbody
2	=	initial afterbody point

Received April 15, 1970; revision received June 29, 1970. This work was partially supported by Contract DA-01-021-AMC-13902(Z) and performed in cooperation with the Aerodynamics Branch of the Research and Engineering Directorate, U. S. Army Missile Command, Redstone Arsenal, Ala.

* Associate Professor of Mechanical Engineering. Member AIAA.

Introduction

DURING powered supersonic flight, base drag due to the interaction between the propulsive-nozzle and freestream flows is a significant part of the over-all drag of a vehicle.[1,2] Two effective techniques for reducing base drag are mass bleed into the base region and/or using a boattailed afterbody. Evaluation of the effects of these techniques on vehicle performance must also consider the tradeoffs involved. For example, when the base-bleed flow is diverted from the propulsive-nozzle stagnation chamber, the gain achieved by base-drag reduction must be considered relative to the thrust that would have been produced if the base-bleed flow had been expanded through the propulsive nozzle. When a boattail is used, the tradeoff between afterbody drag and base drag must be considered. If both techniques are involved, the individual effects and their interaction must be evaluated. As a consequence, the evaluation and possible optimization procedures can be judged best on a unified basis by the relative gain achieved in the thrust-minus-drag force, F_{NET}.[3] Presented herein are the bases for such evaluations and example results for cylindrical and conical afterbodies (Fig. 1). The flowfield over the afterbody is determined by the Method of Characteristics and the base-flow analysis is based on the flow model of Korst, et al.[4] These analyses have been incorporated into computer programs currently available.[5,6]

Analysis

For the control volume of Fig. 1b

$$F_{NET} = \rho_{1I}A_{1I}V_{1I}^2 - \int_{(A_{BT})_X} (P_E - P_{BT})\, d(A_{BT})_X - (P_E - P_B)(A_{1E} - A_{1I}) - (P_E - P_{1I})A_{1I} \quad (1)$$

In Eq. (1), the effects of friction have been neglected and the base-bleed flow, if any, is assumed to possess negligible momentum. Using freestream conditions and the maximum body cross-sectional area as reference quantities, Eq. (1) can be expressed in nondimensional form as

$$F_{NET}/(\rho_E V_E^2 A_{2E}/2) = -C_{DBT} - C_{DB} - [\bar{A}_{1I} - \bar{P}_{1I}\bar{A}_{1I}(1 + \gamma_I M_{1I}^2)]/(\gamma_E M_E^2/2) \quad (2)$$

The boattail and base drag coefficients are defined, respectively, as

$$C_{DBT} = \int_{(\bar{A}_{BT})_X} (1 - \bar{P}_{BT})d(\bar{A}_{BT})_X/(\gamma_E M_E^2/2) \quad (3)$$

and

$$C_{DB} = (1 - \bar{P}_B)(\bar{A}_{1E} - \bar{A}_{1I})/(\gamma_E M_E^2/2) \quad (4)$$

The over-all afterbody-base drag coefficient is

$$C_D = C_{DBT} + C_{DB} \quad (5)$$

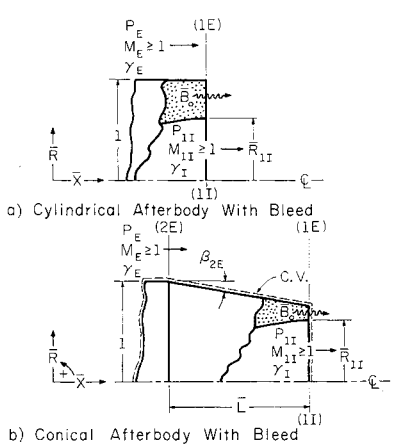

Fig. 1 Configurations and notation.

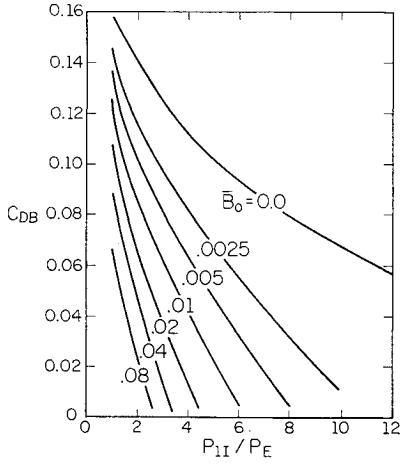

Fig. 2 Variation of the base-drag coefficient with base bleed (cylindrical afterbody).

Choosing the cylindrical afterbody without base-bleed flow as a reference configuration, an incremental thrust-minus-drag force coefficient defined as

$$\Delta C_F = [F_{NET} - (F_{NET})_R]/(\rho_E V_E^2 A_{2E}/2) \quad (6)$$

can be expressed using Eq. (2) as

$$\Delta C_F = -C_{DBT} - [C_{DB} - (C_{DB})_R] + [1 + \gamma_I M_{1I}^2]\bar{A}_{1I}[\bar{P}_{1I} - (\bar{P}_{1I})_R]/(\gamma_E M_E^2/2) \quad (7)$$

For fixed propulsive-nozzle geometry and generating conditions, the diversion of mass flow from the propulsive-nozzle stagnation chamber for base bleed can be expressed by

$$\bar{P}_{1I}/(\bar{P}_{1I})_R = (1 - \bar{B}_0) \quad (8)$$

Combining Eqs. (7) and (8), the result is

$$\Delta C_F = -C_{DBT} - [C_{DB} - (C_{DB})_R] - \bar{B}_0(\bar{P}_{1I})_R\bar{A}_{1I}[1 + \gamma_I M_{1I}^2]/(\gamma_E M_E^2/2) \quad (9)$$

The values of the base and boattail drag coefficients can be determined, e.g., from the aforementioned computer programs[5,6]; the effectiveness of base bleed and/or boattailing can be assessed then by comparing the respective incremental thrust-minus-drag force coefficients determined from Eq. (7) or (9).

Representative Case

The foregoing analysis has been carried out for the representative geometric configurations and flow conditions summarized in Table 1. Detailed afterbody and base-flow solution data[5,6] are available from previous parametric studies of base-flow problems.

For a cylindrical afterbody, the predicted reduction in the base drag cofficient as a result of base-bleed flow is shown in Fig. 2; reductions in the base drag coefficient are achieved, although with progressively less effectiveness, by increasing the base-bleed flow. If no charge is made for the base-bleed flow, ΔC_F is simply equal from Eq. (7) to the difference in base drag coefficients for the bleed and no-bleed cases presented in Fig. 2. When the base-bleed flow is diverted from the propulsive-nozzle stagnation chamber, the behavior of the base drag coefficient is still given by Fig. 2 and the incremental thrust-minus-drag force coefficient determined from Eq. (9) is shown in Fig. 3. In contrast to the former case, the maximum attainable values of ΔC_F are readily apparent from Fig. 3.

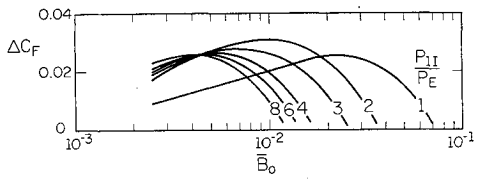

Fig. 3 Variation in the incremental thrust-minus-drag force coefficient due to base-bleed flow diverted from the propulsive-nozzle stagnation chamber (cylindrical afterbody).

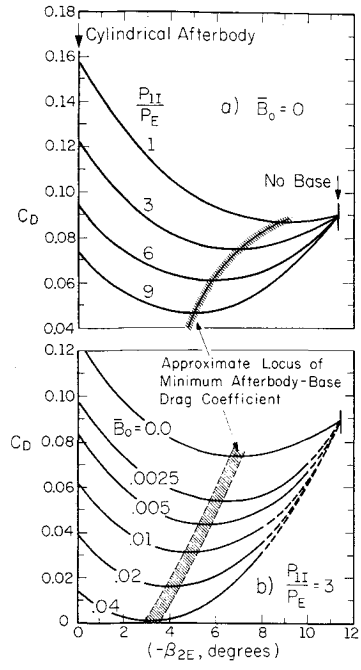

Fig. 4 Afterbody-base drag coefficient for a) several operating pressure ratios without base-bleed flow and b) several base-bleed flows at a fixed operating pressure ratio (conical boattail, $\bar{L}$ = 2).

Figure 4a demonstrates the dependence of the over-all afterbody-base drag coefficient C_D on the conical-boattail angle β for several operating pressure ratios and no base-bleed flow. For a given operating pressure ratio, C_D can be minimized by the proper selection of β; the locus of these minimum values of C_D is also indicated in Fig. 4a. The influence of base-bleed flow for this configuration can be demonstrated best for a fixed operating pressure ratio; the functional behavior and the possible minimization of C_D are shown in Fig. 4b for an operating pressure ratio of P_{1I}/P_E = 3 and parametric values of the base-bleed flow ratio. Thus, the possibility of reducing and minimizing the base drag coefficient by proper selection of a conical-boattail angle and base-bleed flow-rate ratio is demonstrated in Fig. 4.

For diversion of the base-bleed flow of Fig. 4b from the propulsive-nozzle stagnation chamber, Fig. 5 clearly demonstrates the potential gains in ΔC_F that could be achieved with both boattailing and base-bleed flow. For this operating condition, ΔC_F can be maximized by proper selection of the conical-boattail angle and base-bleed flow-rate ratio; the locus of these maximum values is given in Fig. 5. A noteworthy point, from Fig. 5, is the significant potential gains in ΔC_F

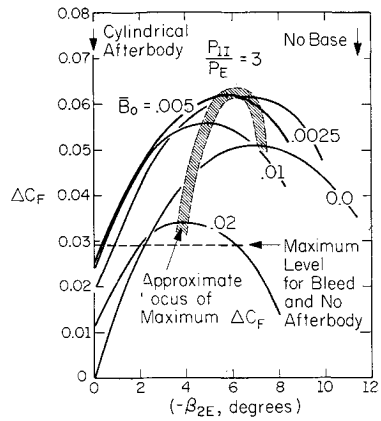

Fig. 5 Variation in ΔC_F due to base-bleed flow diverted from the propulsive-nozzle stagnation chamber at a fixed operating pressure ratio (conical boattail, $\bar{L}$ = 2).

Table 1 Summary configuration and flow data

Conical boattail		Base-flow variables									
$\bar{L}$	$-\beta_{2E}$	$\bar{X}_{1I}$	$\bar{R}_{1I}$	β_{1I}	γ_I	M_{1I}	$\bar{X}_{1E}$	$\bar{R}_{1E}$	γ_E	M_{1E}	$\mathcal{R}_1$	$\bar{T}_{0E}$
2	0–11.309	0	0.6	0°	1.4	2.5	0	1–0.6	1.4	2	1	1

that can be achieved with combined base bleed and boattailing as compared to base bleed only.

The foregoing results, which were presented to demonstrate the optimization and evaluation techniques, have been limited to a single boattail geometry and length, as well as a limited operating pressure range. However, these results are representative of the data which can be generated readily with existing computer programs[5,6] and of the bases for optimization and appraisal of over-all system performance.

References

[1] Sedney, R., "Review of Base Drag," *The Fluid Dynamic Aspects of Ballistics*, NATO-AGARD CP 10, Paris, France, Sept. 1966, pp. 211–240.

[2] Brazzel, C. E. and Henderson, J. H., "An Empirical Technique for Estimating Power-On Base Drag of Bodies-of-Revolution with a Single Jet Exhaust," *The Fluid Dynamic Aspects of Ballistics*, NATO-AGARD CP 10, Paris, France, Sept. 1966, pp. 241–261.

[3] Korst, H. H., Addy, A. L., and Chow, W. L., "Installed Performance of Air-Augmented Nozzles Based on Analytical Determination of Internal Ejector Characteristics," *Journal of Aircraft*, Vol. 3, No. 6, Nov.–Dec. 1966, pp. 498–506.

[4] Korst, H. H., Chow, W. L., and Zumwalt, G. W., "Research on Transonic and Supersonic Flow of a Real Fluid at Abrupt Increases in Cross Section (with Special Consideration of Base Drag Problems)—Final Report," ME-TN 392-5, Dec. 1959, Univ. of Illinois, Urbana, Ill.

[5] Addy, A. L., "Analysis of the Axisymmetric Base-Pressure and Base-Temperature Problem with Supersonic Interacting Freestream-Nozzle Flows Based on the Flow Model of Korst, et al., Part I: A Computer Program and Representative Results for Cylindrical Afterbodies," RD-TR-69-12, July 1969, U.S. Army Missile Command, Redstone Arsenal, Ala.

[6] Addy, A. L., "Analysis of the Axisymmetric Base-Pressure and Base-Temperature Problem with Supersonic Interacting Freestream-Nozzle Flows Based on the Flow Model of Korst, et al., Part III: A Computer Program and Representative Results for Cylindrical, Boattailed, or Flared Afterbodies," RD-TR-69-14, Feb. 1970, U.S. Army Missile Command, Redstone Arsenal, Ala.

Machine-Aided Photo Interpretation Techniques for Vegetation Analysis

J. D. LENT* AND J. D. NICHOLS†

School of Forestry and Conservation, University of California, Berkeley, Calif.

LARGE-SCALE "operational" survey missions, using Earth-orbital satellite sensing platforms, are planned to begin as early as 1972. Efficient data handling schemes are needed to keep pace with the rates at which such missions can collect and subsequently return or transmit remotely sensed data. This Note explores some of the capabilities which various remote sensing systems offer, in terms of spatial resolution and user requirements, for obtaining rapid land-use inventories.

Presented as Paper 70-308 at the AIAA Earth Resources Observations and Information Systems Meeting, Annapolis, Md., March 2–4, 1970; submitted March 17, 1970; revision received May 26, 1970.

* Associate Specialist.

† Project Engineer.

Desired Inventory Information and Sensor Resolutions

With respect to vegetation-oriented resource inventories in the U.S., the land-use manager is mainly concerned with four broad categories: agricultural crops, forests, rangelands, and brushlands. The following lists of desired information for these categories suggest a need to examine spatial resolution requirements at the various possible remote sensing altitudes and corresponding sensor resolution capabilities.

Agricultural crops

For land-use inventory purposes, the following information, as a minimum, is desired at relatively frequent intervals: 1) total crop acreage by growing region, 2) acreage per crop type, by growing region, 3) state of vegetational maturity and yield, and 4) extent of crop-damaging agents, per crop type and by source for all growing regions.

Forests

The following data are desired, but at much less frequent intervals: 1) total forest acreage, 2) acreages of commercial vs noncommercial forests, 3) forest stand vigor and volume, per species and size class (commercial stands only), 4) predictable future volume yield, per species and size class (commercial forest stands only), and 5) extent of tree-damaging agents, per forest type and size class (commercial forest stands, primarily).

Rangelands

The following information is desirable, as a minimum, at infrequent prescribable intervals: 1) total acreage, 2) compositional structure of tracts in terms of animal "carrying capacity," 3) present and probable future animal carrying capacity, and 4) extent of range-damaging agents or causes (weeds, rodents, drought, etc.)

Brushlands

The following data are desirable at very infrequent intervals: 1) total acreage, 2) acreages of various brushland types, and 3) vegetative density, by type. (More specific brushland information will depend upon the primary importance of the vegetation to such uses as watershed protection, wildlife habitat, or potential conversion to forest stands, agriculture sites, recreation, etc.)

The proposed "operation" Earth resource technology satellite ERTS-A, which is scheduled for launch in March 1972, reveals fairly coarse resolution capabilities in terms of the total vegetation inventory data requirements. It will possess ground resolution capabilities ranging from 200–500 ft at the proposed orbital altitude of 496 naut miles. One of the sensors, an optical-mechanical scanning device, will have four-channel recording capability ranging in sensitivity from the blue-green to the near infrared wavelength intervals of the electromagnetic spectrum. The second sensor, a three-channel return beam vidicon system (RBVS), will record radiant wavelength energy from the blue-green through the red portion of the electromagnetic spectrum. The recorded data will be transmitted to various ground stations and subsequently transcribed to film emulsions for image analysis. These same data can remain in digital form for machine-aided interpretation as well. Due to the spatial resolution capability which this initial satellite sensor package will possess, it is suggested that general land-use classifications can be performed adequately. Note that when high-resolution films are used to sense and record the data (which is proposed in the follow-on ERTS-B and C satellites), considerably more information can be extracted. Such films possess a spatial resolution capability which will be at least one-order of magnitude better than that described previously for the ERTS-A sensors.